引用格式：JIANG Xiaowei, WANG Sheng, WU Hua. Metamaterial Absorber with Tunable Absorption Bandwidth Based on Vanadium Dioxide[J]. Acta Photonica Sinica, 2022, 51(1):0151124
江孝伟,王胜,武华.基于二氧化钒的吸收带宽可调谐超材料吸收器[J].光子学报,2022,51(1):0151124

基于二氧化钒的吸收带宽可调谐超材料吸收器

江孝伟[1,3],王胜[1],武华[2,3]
(1 衢州职业技术学院 信息工程学院,浙江 衢州 324000)
(2 赣南师范大学 物理与电子信息学院,江西 赣州 341000)
(3 北京工业大学 光电子技术教育部重点实验室,北京 100124)

摘 要:提出了一种由二氧化钒(VO_2)和金属Au构成的吸收带宽可调谐的超材料完美吸收器(MPA)。模拟发现,该MPA的吸收波长覆盖了可见光和近红外光。改变VO_2温度,MPA的吸收带宽可实现0.378 μm的调谐。分析MPA在吸收波长处的磁场分布发现MPA激发了表面等离子激元共振,实现在可见光和近红外光完美吸收。本文提出的MPA可应用于智能设备和热发射器等当中。

关键词:超材料;吸收器;可调谐带宽;二氧化钒;表面等离子激元
中图分类号:O436 **文献标识码**:A **doi**:10.3788/gzxb20225101.0151124

0 Introduction

Adjusting the Metamaterial (MM) cell resonance structure may show many exotic electromagnetic properties, such as negative refraction[1-2], perfect absorption[3-4], electromagnetic stealth[5-6], and electromagnetic induction transparency[7]. Because MM has the above-mentioned abnormal electromagnetic properties, it has gradually become a research hotspot, and has been widely used in national defense, communications, and biomedical sensing[8-10].

The Metamaterial Perfect Absorber (MPA) has attracted widespread attention due to unprecedented characteristics compared to taper-like structure absorbers[11] or ordinary absorbers, such as high absorption efficiency, ultrathin thickness, and a scalable working wavelength[12]. Since Landy et al. first proposed an MPA with perfect absorption characteristics[3], different types of MPAs have been proposed, and the absorption wavelengths over microwave[13], terahertz[14], infrared,[15] and visible bands have been identified[16]. However, once the structural parameters of MPAs are fixed, their absorption characteristics are difficult to be tuned. On the other hand, demand on tunable MPA is increasing in many applications, such as modulators, optical switches, and smart reflectors.[17].

To realize the dynamic tunability of the absorption characteristics of MPA, many research groups choose to incorporate varactor diodes or graphene into the design of MPA. In the low-frequency band, diodes with changeable capacitance are generally used to change the equivalent capacitance of MPA to achieve dynamic tuning of MPA absorption wavelength and absorption efficiency[18-19]. In the high-frequency band, graphene is used in MPA. By changing the chemical potential of graphene, one can achieve dynamic control of absorption wavelength, absorption efficiency, and even absorption bandwidth of MPAs[20-21].

In recent years, phase-changing material vanadium dioxide (VO_2) demonstrated outstanding optical and

Foundation item: National Natural Science Foundation of China (Nos. 61575008, 61650404), the Public Welfare Technology Research Project of Zhejiang Province (No. LGC21E050002), the Quzhou Science and Technology Project (No. 2019K20)
First author: JIANG Xiaowei (1991—), male, lecturer, M.S. degree, mainly focuses on the theory and preparation of metamaterial devices. Email: JosephJiangquzhi@126.com
Contact author: WANG Sheng (1985—), male, associate professor, M.S. degree, mainly focuses on the optoelectronic devices. Email: 158942287@qq.com
Received: Jun.25,2021; **Accepted**: Sep.2,2021

electrical properties, and can realize the transition between metallic state and dielectric state through external excitations, such as light, electricity, and heat[22-23]. Because VO_2 has reversible phase-changing characteristics, it is an ideal material for preparing a tunable MPA, and many research work has been done on tunable MPAs based on VO_2. LEI L et al from Shenzhen University designed an absorption-bandwidth-tunable MPA based on VO_2 and metallic chromium materials[24]. DAO Rina et al from Nanjing University of Posts and Telecommunications used VO_2 as a resonance unit material, and the absorption efficiency of MPA could be tuned by changing the temperature of the resonance unit [25]. Our research group also demonstrated tunable absorption wavelength and absorption efficiency of MPA by using VO_2 and graphene in MPA[26].

To the best of our knowledge, current VO_2-based MPA can realize tunable absorption efficiency, but the tuning of absorption bandwidth is rarely involved. Moreover, the tunable MPA bandwidth in visible and near-infrared bands is even less involved. However, at present, for the application of intelligent windows, intelligent reflectors, intelligent temperature control systems, and heat emitters, MPA absorption bandwidth is required to be tunable in the visible and near-infrared bands[27-28]. Therefore, in this paper, a bandwidth-tunable VO_2-based MPA in visible and near-infrared bands is proposed and studied using Finite Difference Time Domain (FDTD) method. The simulation results showed that the bandwidth, $W_{a,}$ of the tunable MPA proposed in this paper could reach 1.03 μm and 0.652 μm with absorption efficiency higher than 90% in the VO_2 dielectric and metallic state. By analyzing the electromagnetic field distribution of MPA, it was observed that as VO_2 was in the dielectric state, MPA achieved a wide bandwidth and high absorption owing to the Propagating Surface Plasmon (PSP), Localized Surface Plasmon (LSP), and the resonance of Fabry-Perot (FP) cavity.

1 Device structure and theory

The structure of the absorption-bandwidth-tunable MPA is shown in Fig. 1. Fig. 1 (a) is overall view of the MPA structure, and Fig.1 (b) is zoom-in view of one MPA unit cell. The MPA unit cell is composed of an Au substrate and four cylindrical resonance units with different radii. The cylindrical resonance units are of two-layered structure, with VO_2 as bottom layer and Au as top layer. The structural parameters are as follows: P is the period of the MPA unit cell; r_1, r_2, $r_{3,}$ and r_4 are the radii of the four cylindrical resonance units respectively; h_m=0.03 μm and h_v=0.11 μm are the thickness of Au and VO_2 in the cylindrical resonance unit respectively; w_1, w_2, w_3 and w_4 are spacing between different cylinder resonant elements. In this work, the thickness of the Au substrate is 0.2 μm, which is thick enough to block the incident light effectively, and the transmission of the structure is nearly zero.

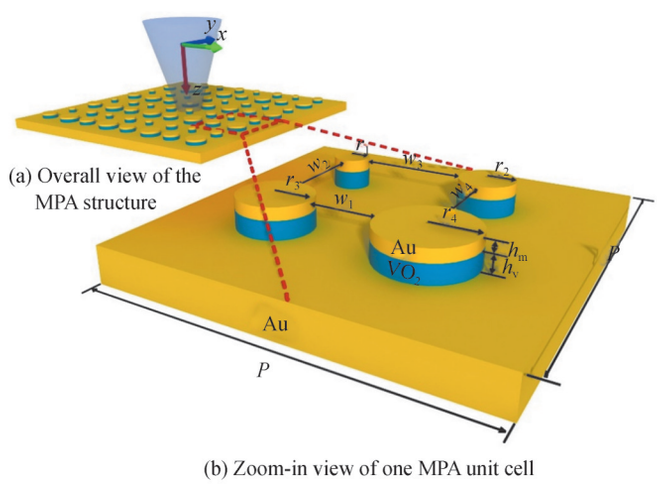

Fig. 1 schematic of the structure of absorption-bandwidth-tunable MPA

With the development of material preparation technology and nanofabrication technology, the current micro-nano machining technology can fully meet the requirements of MPA processing as shown in Fig. 1. Therefore, the MPA structure proposed in this paper is easier to realize in an actual experiment. The proposed structure in Fig.1 can easily be realized by current nano-fabrication technology. Firstly, a continuous VO_2 layer is prepared on the Au substrate by the lower-cost sol-gel method [29], then a thin Au layer was sputtered on the

VO_2 layer by magnetron sputtering, finally the required cylindrical resonance units are patterned by electron beam lithography and ion beam etching.

The refractive index n, and coefficient k of Au for different light wavelengths could be obtained from Ref. [30], as shown in Fig. 2. According to the Bruggeman's effective medium theory[31], The dielectric constant of VO_2 could be calculated by Eq. (1). In Eq. (1), $\varepsilon_i \approx 9$ is the dielectric constant of VO_2 in the dielectric state, ε_m is the dielectric constant of VO_2 in the metallic state, and f represents the volume ratio of VO_2 in the metallic state in the entire VO_2. Moreover, ε_m could be obtained by Eq. (2). In Eq. (2), ω_p is the plasma frequency, ω is the incident light angular frequency, $\tau = 2\ \mu m_e/e$ is the relaxation time, m_e is the mass of free electrons, $u \approx 2\ cm^2/V$. s is carrier mobility, and e is the amount of free electron charge. Furthermore, f could be obtained by Eq. (3), where T represents the environment temperature, $T_0 = 68^\circ C$ represents the VO_2 phase transition temperature, and $\Delta T = 6^\circ C$ is the transition width. Eqs. (1)~(3) could be combined to obtain the refractive index, n_{VO_2}, and the extinction coefficient, k_{VO_2}, of VO_2 for different wavelengths at different temperatures, as shown in Fig. 3.

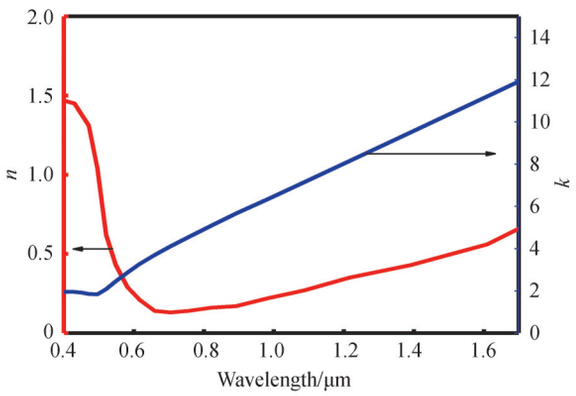

Fig. 2 Refractive index and extinction coefficient of Au

$$\varepsilon_{VO_2} = \frac{1}{4}\{\varepsilon_i(2-3f)+\varepsilon_m(3f-1)+\sqrt{[\varepsilon_i(2-3f)+\varepsilon_m(3f-1)]^2+8\varepsilon_i\varepsilon_m}\} \tag{1}$$

$$\varepsilon_m(\omega) = \varepsilon_i + i\frac{\omega_p^2}{\omega(\omega + i/\tau)} \tag{2}$$

$$f = 1 - \frac{1}{1+\exp[(T-T_0)/\Delta T]} \tag{3}$$

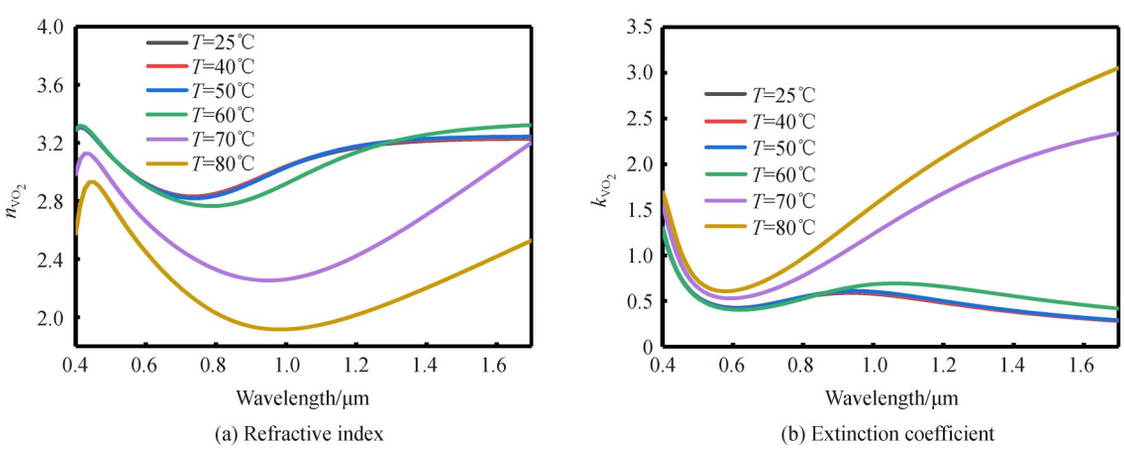

Fig. 3 Refractive index and extinction coefficient of VO_2 at different temperatures

2 Results and discussions

The characteristics of proposed MPA is studied by FDTD simulation. Since the MPA is of periodic structure, by carefully setting boundary conditions, it is feasible to only simulate the unit structure as shown in Fig. 1(b) in FDTD software. A periodic boundary condition was added in the x- and y-directions. A perfect match layer was added in the z-direction as the boundary condition. The polarization of the incident light was set to be TM polarization (Along the x axis). Incident light was perpendicular to the surface of the structure, which indicated the incident angle θ is 0. To ensure that the simulation results were closer to reality, the grid type was

auto non-uniform during simulation, and the grid accuracy was set to the maximum value of 8. The details are shown in Fig. 4.

Fig. 5 shows FDTD simulation results of absorption spectra of MPA at different temperatures. As Fig. 5 shows, at T=80°C, the MPA could maintain more than 90% absorption efficiency between 0.505 μm and 1.157 μm, and the absorption bandwidth W_a could reach 0.652 μm. When the temperature T dropped from 80°C to 25°C, the MPA could maintain more than 90% absorption efficiency between 0.505 μm and 1.535 μm, and the absorption bandwidth, W_a reached 1.03 μm. These findings indicate that the MPA proposed in this paper can realize the tuning of absorption bandwidth by changing the VO_2 temperature, and the tuning range of absorption bandwidth can reach 0.378 μm. In addition, the results show that the absorption spectrum of MPA covers both the visible and near-infrared bands.

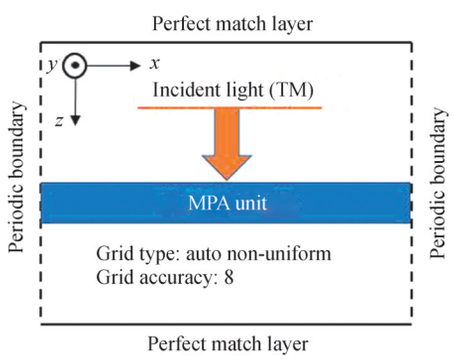

Fig.4 Detailed settings of the FDTD simulation

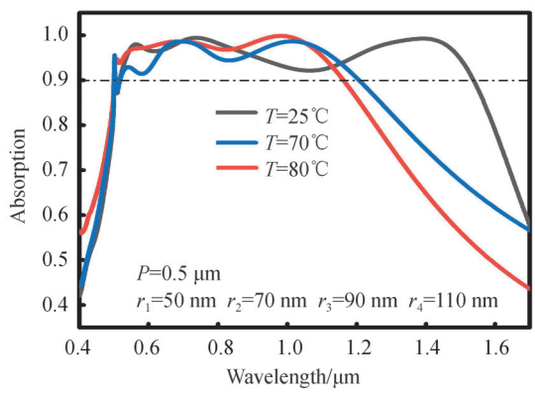

Fig. 5 Absorption as a function of wavelength of MPA at different temperature

To explore the internal physical mechanism of the MPA with tunable absorption bandwidth, the electromagnetic field distribution of MPA at different resonance wavelengths is simulated and calculated at low temperature. Fig. 6 shows the electric field distribution of MPA in the $x-z$ plane ($y=-0.125$ μm, e.g. the center plane of cylinders with radii r_3 and r_4) under different resonance wavelength conditions (T=25°C). As shown in Fig. 6, under different resonance wavelength conditions, the electric field is basically concentrated between the gaps of the cylindrical resonance units and the corners of the Au cylinder, which indicates the incident light excites the surface plasmon polaritons (SPPs) in the MPA. Therefore, from the electric field distribution, it can be concluded that the high absorption of the MPA at each resonance wavelength is due to SPP resonance[24].

Unlike the electric field distribution, the magnetic field distribution (T=25°C) of the MPA under different resonance wavelength conditions is very different. As shown in Fig. 7(a) and 7(b), LSP resonance is the

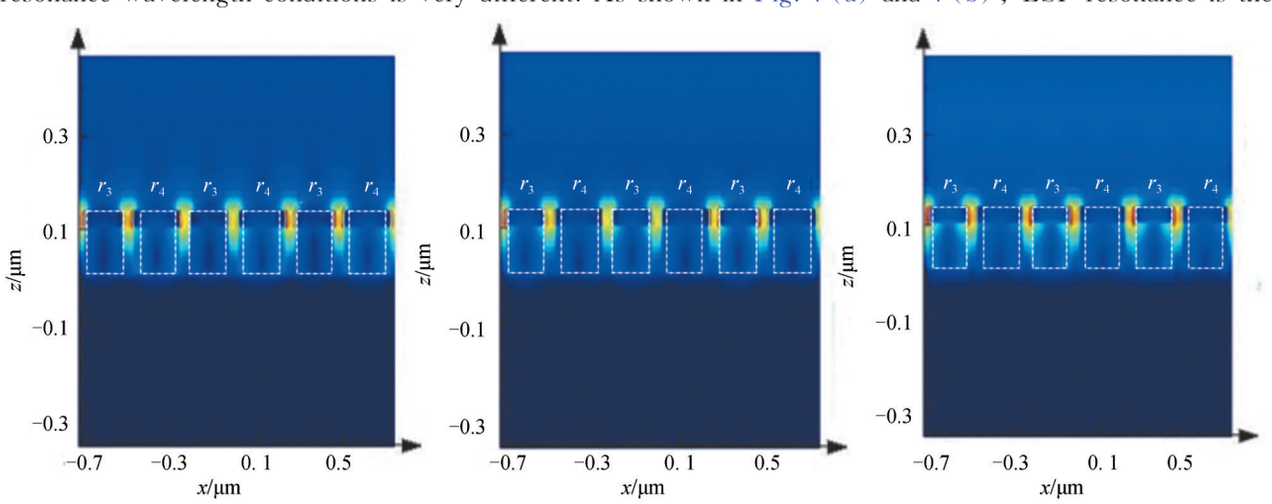

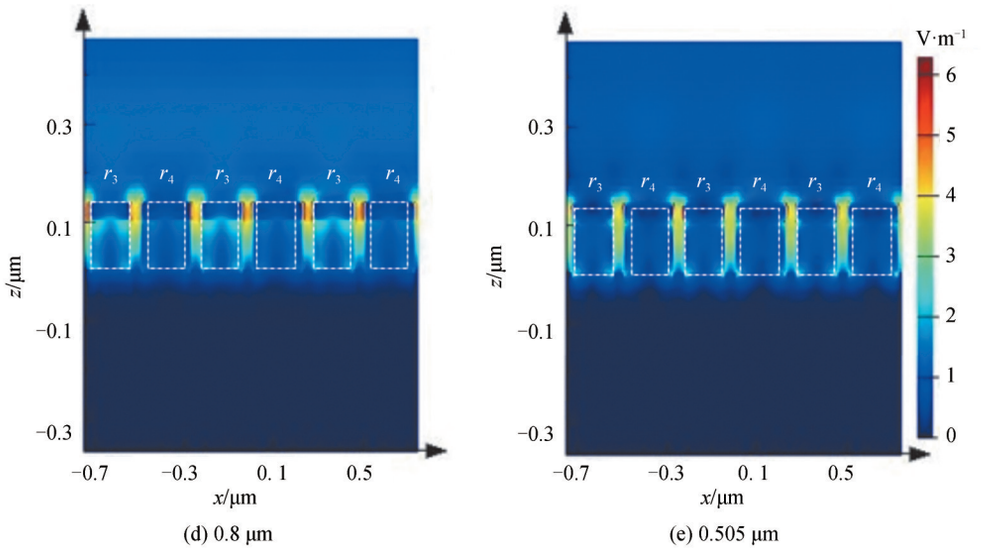

Fig. 6 Electric field distribution of MPA at the different resonance wavelength (T=25℃)

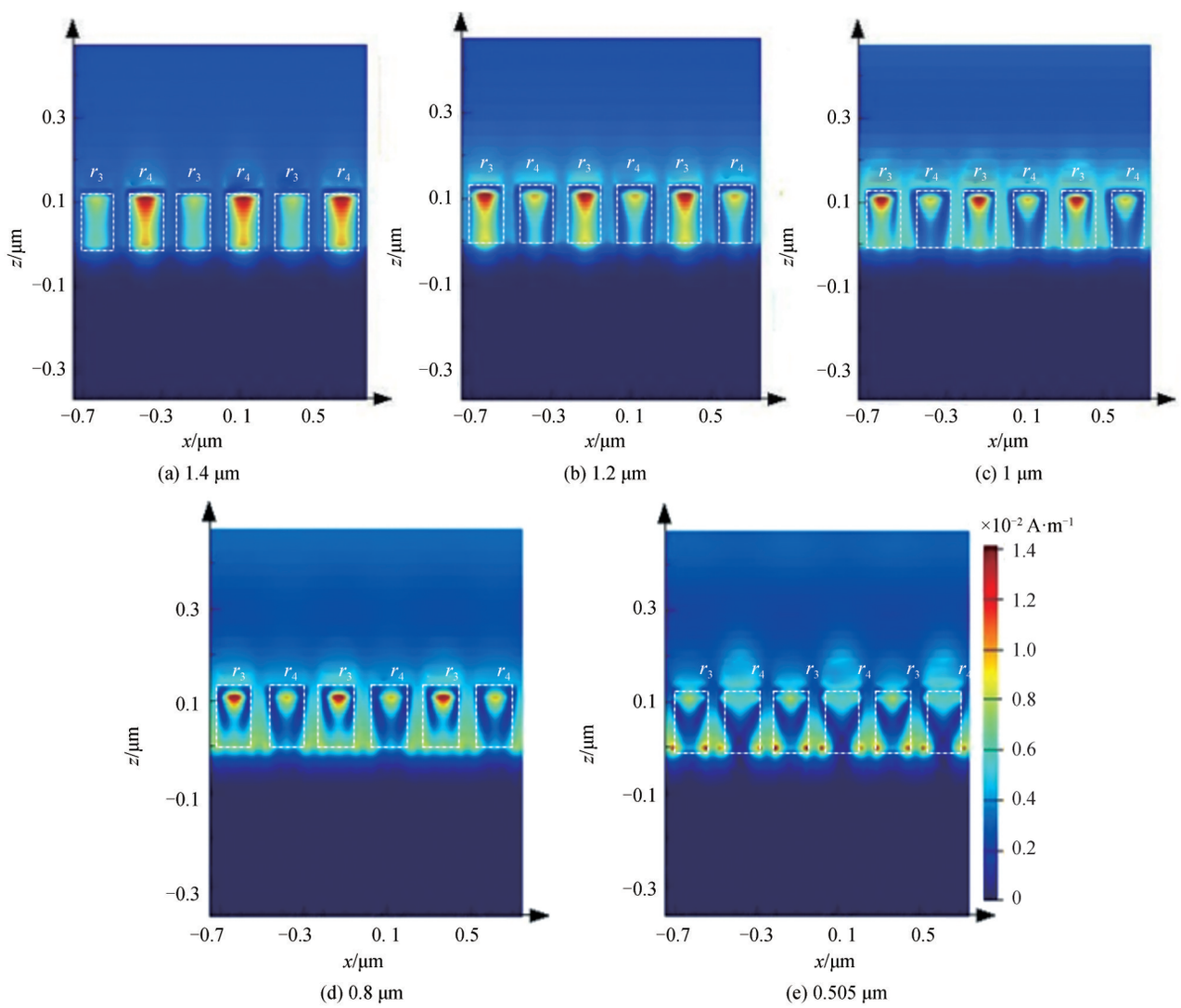

Fig. 7 The magnetic field distribution of MPA at the different resonance wavelength (T=25℃)

mainreason for the high absorption efficiency of MPA at long wavelengths (1.4 μm and 1.2 μm). Moreover, most of the magnetic field is confined to the VO_2 layer, which is between the Au cylinder and the Au substrate[23]. Fig. 7(e) shows that the high absorption efficiency of MPA at a short wavelength (0.505 μm) is mainly due to PSP resonance, because only a small part of the magnetic field is restricted to the VO_2 layer, and most of magnetic field is located between adjacent cylindrical resonance units, which is a significant PSP resonance feature[32-33]. The specific proof can also be seen in Fig. 9(a). As for the resonance absorption of MPA at wavelengths of 0.8 μm and 1 μm, Fig. 7(c) and 7(d) show that it is not only caused by LSP resonance and PSP resonance, but is also mixed with FP cavity resonance, that is, the light wave oscillated back and forth between the Au cylindrical layer and the Au substrate. In this case, the Au cylindrical layer and Au substrate act as mirrors to form a FP resonator.

To understand the intrinsic physical mechanism of the high absorptivity of MPA in the VO_2 metallic state, the electromagnetic field distribution of MPA at the wavelength of 0.505 μm and 1 μm at T=80℃ is calculated, as shown in Fig. 8. Fig. 8(a) shows the magnetic field distribution of the MPA at a wavelength of 0.505 μm. Compared with Fig. 7(e), the magnetic field distribution of VO_2 at the short wavelength is basically the same regardless of whether VO_2 is in the dielectric state or metallic state. That is, the physical mechanism leading to the high absorption efficiency of MPA at the short wavelength is the same, which is because of the PSP resonance.

Comparing Fig. 8(b) with Fig. 7(c), it can be seen that when VO_2 is in the metallic state, the high absorption efficiency of MPA at long wavelengths (1 μm) is not only caused by LSP or PSP resonance, but

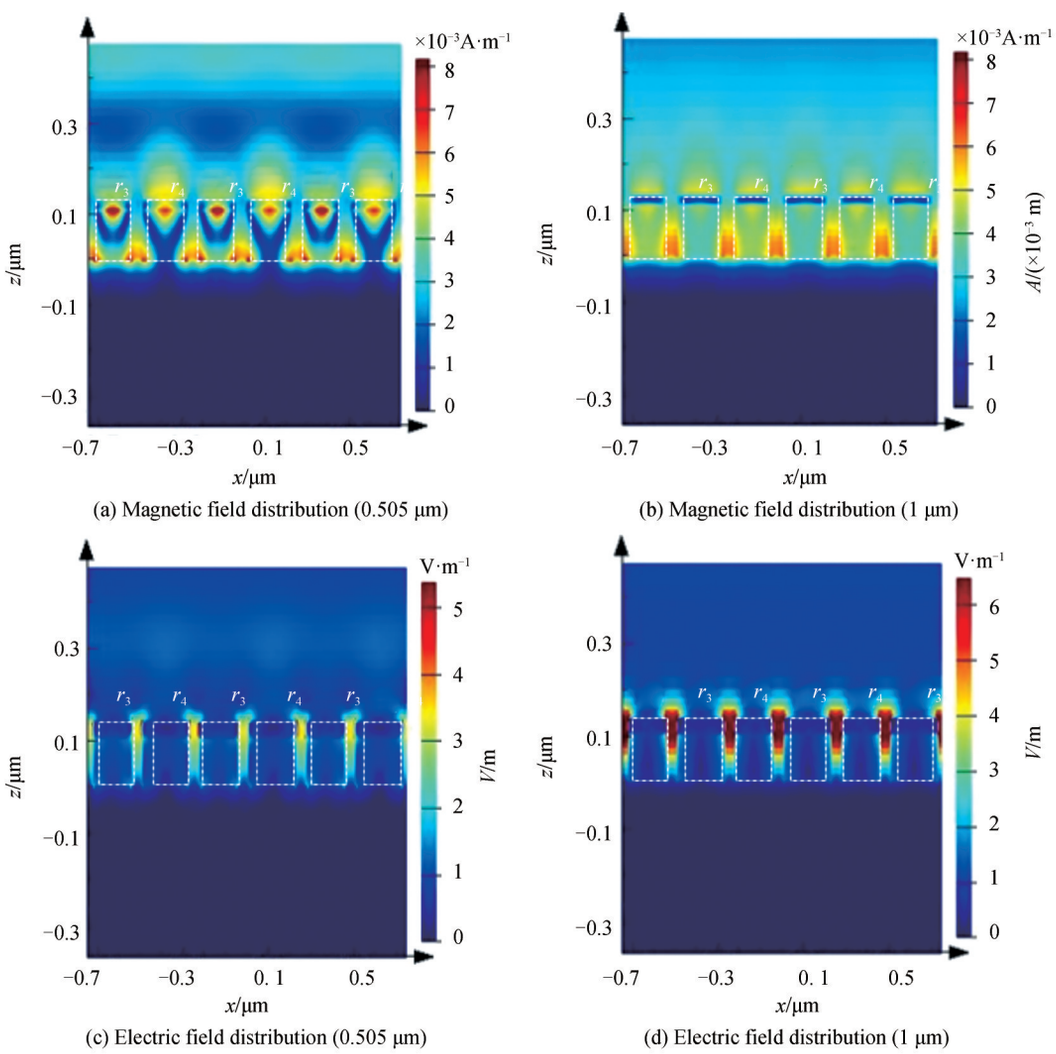

(a) Magnetic field distribution (0.505 μm)　(b) Magnetic field distribution (1 μm)

(c) Electric field distribution (0.505 μm)　(d) Electric field distribution (1 μm)

Fig. 8　The electromagnetic field distribution of MPA at resonance wavelength (T=80℃)

also mainly because of FP cavity resonance. The FP cavity resonance here is mainly composed of an adjacent cylinder resonance units and air gap [24]. The FP cavity length is the thickness of cylinder resonance unit (h_m+h_v). The width of FP cavity is w_1. Owing to the formation of the FP cavity, more magnetic fields are concentrated between the air gaps of the adjacent cylinder resonance units. Figs. 8(c) and 8(d) show the electric field distribution of MPA at a wavelength of 0.505 μm and 1 μm when VO_2 is in a metallic state, respectively. It can be seen the high absorption efficiency of MPA at high temperature is also due to the SPP resonance.

To explore the influence of MPA structural parameters on its absorption characteristics at low temperature (VO_2 is in dielectric state, T=25℃), the MPA absorption spectra (T=25℃) under the conditions of different periods P and cylindrical resonance unit radius were simulated and calculated. Fig. 9(a) shows the influence of P on the absorption spectrum of MPA. As P increased, the absorption bandwidth of MPA gradually narrowed, and the absorption wavelength of MPA at the short-wavelength gradually showed redshift. When P increased from 0.5 μm to 0.6 μm, the initial wavelength of the MPA absorption spectrum shifted from 0.505 μm to 0.599 μm. It can be found that the absorption wavelength of MPA at short wavelengths is very close to P. This phenomenon is due to the fact that high absorption efficiency of MPA at short wavelengths is caused by PSP resonance. The PSP resonance wavelength, λ_{PSP}, is related to the MPA period, P, which can be seen in Eq. (4) [32]. In Eq. (4), m is an integer, λ_0 is the free-space wavelength. Because the incident light is perpendicular to the surface of the MPA, θ is 0, therefore λ_{PSP} equals to P.

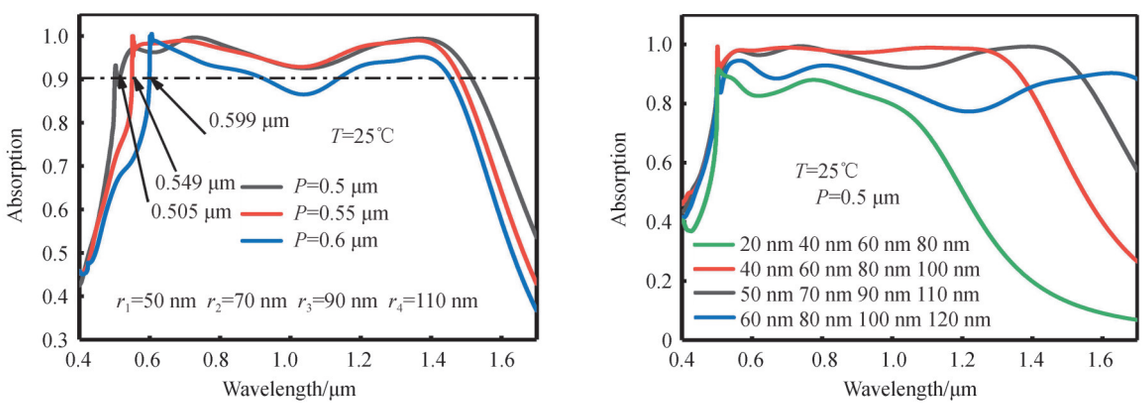

(a) The influence of P on the absorption spectrum

(b) The effect of the radius of resonance element on the absorption spectrum

Fig.9 The influence of MPA structural parameters on the absorption spectrum of MPA (T=25℃)

As Fig. 9(a) shows, although the P of MPA gradually increased, there is no obvious redshift or blueshift at the MPA wavelength of 1.4 μm. This is because, as can be seen from Fig. 7(a), the high absorption efficiency of MPA at 1.4 μm is caused by LSP resonance, and period P has almost no effect on the LSP resonance wavelength.

$$\frac{1}{\lambda_{PSP}}=\frac{1}{\lambda_0}\sin\theta+\frac{m}{P} \tag{4}$$

Fig. 9(b) shows the MPA absorption spectra versus the radii of different cylindrical resonance units. As can be seen from Fig. 9(b), with an increase in the radius of the resonance unit, the MPA absorption bandwidth, W_a, increased firstly and then decreased. In the short wavelength range between 0.5 μm and 1 μm, in all the 4 simulated conditions, the MPA could maintain a relatively high absorption efficiency (>75%). The reason for this is that the high absorption efficiency of MPA at short wavelength is caused by the PSP resonance, as shown in Fig. 7(e). From Eq. (4), we know the resonance wavelength of PSP is mainly determined by the period P, so as long as P did not change, the MPA could maintain the PSP resonance at the short wavelength. However, the absorption efficiency varied greatly at long wavelengths (>1 μm). The reason for this is that the high absorption efficiency of MPA at long wavelength is caused by LSP resonance, as shown in Fig.7(a) and 7(b). According to Ref. [32], LSP resonance is mainly affected by the shape and size of the MPA resonance unit. Therefore, when the radius of the resonance unit is small, the absorption efficiency of

MPA is extremely low because it cannot meet the conditions to excite LSP resonance; when the radius of the resonance element increases, it gradually meets the excitation conditions of LSP resonance, and increases the absorption efficiency of MPA at the long-wavelength range.

In order to understand the influence of structural parameters on the absorption characteristics of MPA at high temperature (VO_2 is in metallic state, T=80℃), we changed the thickness of top Au layer h_m and the radius of the resonance units. Fig. 10(a) shows the influence of h_m on the absorption characteristics of MPA as VO_2 is in metallic state (T=80℃). As can be seen from Fig. 10(a), when h_m increases, the absorption wavelength of MPA at short wavelength almost unchanged, but the absorption efficiency gradually declines. Refer to Fig. 8(a), when VO_2 is in metallic state, the high absorption efficiency of MPA at the short wavelength is caused by the PSP resonance. On the contrary, the absorption wavelength of MPA in the long wavelength is red-shifted. This is because when VO_2 is the metallic state (T=80℃), the high absorption efficiency of MPA at the long wavelength is due to the FP cavity resonance rather than LSP resonance. The

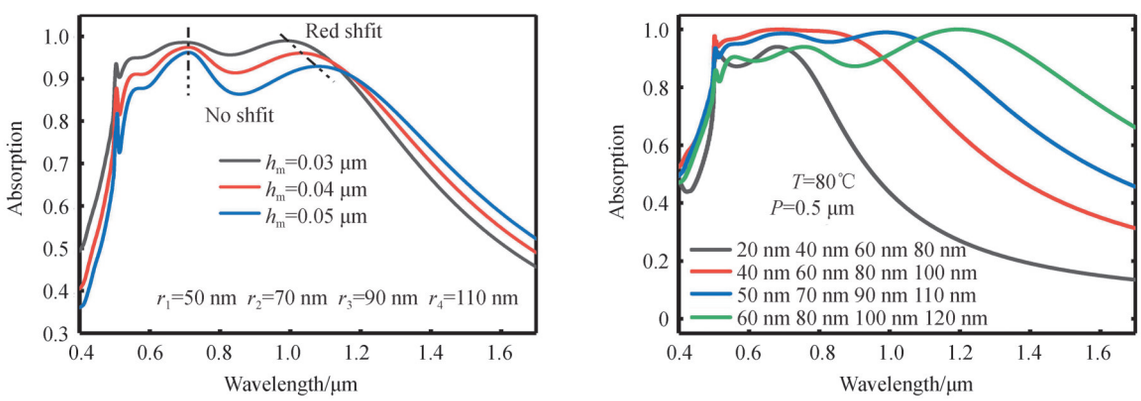

(a) The influence of hm on the absorption spectrum

(b) The effect of the radius of resonance element on the absorption spectrum

Fig.10 The influence of MPA structural parameters on the absorption spectrum of MPA (T=80℃)

relationship between the FP cavity resonance wavelength λ_{FP} and h_m is shown in Eq. (5)[34], where n_{eff} is the FP cavity effective refractive index. According to Eq. (5), with the increase of h_m, the resonant wavelength of FP cavity λ_{FP} will increase, resulting in the red shift of MPA at the long wavelength.

$$\lambda_{FP}=2(h_v+h_m)n_{eff} \tag{5}$$

Fig. 10(b) shows the influence of the MPA resonance unit radius on the absorption characteristics of the MPA. Different from VO_2 in dielectric state, when VO_2 is in metallic state, the absorption efficiency of MPA at long wavelength gradually increases with the increase of the resonance unit radius. As comparison, when VO_2 is in dielectric state, as shown in Fig. 9(b), with the increase of the resonance unit radius, the absorption efficiency of MPA at long wavelength first increases and then decreases. This is mainly because when VO_2 is metallic state, the high absorption efficiency of MPA at long wavelength is due to the FP cavity resonance. With the increase of resonance unit radius, the FP equivalent refractive index gradually meets the resonance condition of long wavelength (see Fig. 11), so that the absorption efficiency of MPA at long wavelength is gradually improved.

The relationship between the width of FP cavity w and the equivalent refractive index of FP cavity n_{eff} can be obtained by Eqs. (6)~(8). ε_m and ε_d=1 are the dielectric constants of Au and air respectively. $k_0=2\pi/\lambda$, where λ is the incident light wavelength. Fig. 11 shows the relationship between w and n_{eff} when the wavelength of incident light is 1 μm ($\varepsilon_m=-47.84+3.11i$). It can be seen from Fig. 11 that as w decreases, that is, as the radius of the cylinder resonance unit increases, n_{eff} will gradually increase. Because the length of the FP cavity unchanged, the resonance wavelength λ_{FP} of the FP cavity will increase when the n_{eff} increases. Therefore, as shown in Fig. 10(b), when the radius of the cylindrical resonance unit increases, the absorption efficiency of MPA at the long wavelength increases.

$$k_{\mathrm{d}}\varepsilon_{\mathrm{m}}\tanh\left(\frac{k_{\mathrm{d}}w}{2}\right)+k_{\mathrm{m}}\varepsilon_{\mathrm{d}}=0 \tag{6}$$

$$k_{\mathrm{d}}=k_0\sqrt{n_{\mathrm{eff}}^2-\varepsilon_{\mathrm{d}}} \tag{7}$$

$$k_{\mathrm{m}}=k_0\sqrt{n_{\mathrm{eff}}^2-\varepsilon_{\mathrm{m}}} \tag{8}$$

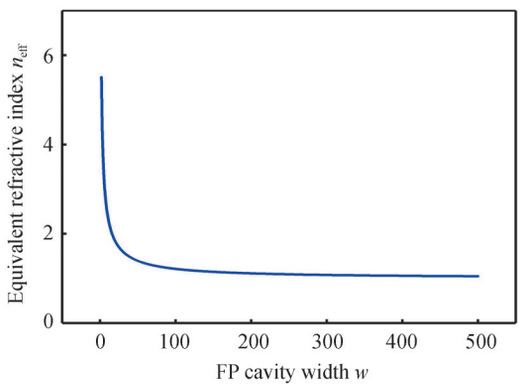

Fig.11 The influence of FP cavity wdith w on the FP cavity equivalent refractive index n_{eff}

3 Conclusions

We designed a MPA with high absorption efficiency and tunable absorption bandwidth in visible and near-infrared light bands. The simulation results indicate that by changing temperature, the absorption bandwidth W_a of the MPA can be tuned, and the tuning range can reach 0.375 μm. We also studied the effects of structural parameters on absorption bandwidth. By analyzing the electromagnetic field of the MPA at absorption wavelength, it can be found that when VO_2 is at a low temperature (T=25°C), the high absorption efficiency of the MPA in the near-infrared band is due to LSP resonance, and the high absorption efficiency of the MPA in the visible band is due to the PSP resonance. However, when VO_2 is at high temperature, the high absorption efficiency of the MPA in the near-infrared band is caused by FP resonance. The research in this paper can provide a theoretical basis for design and fabrication of a high-performance, dynamic, adjustable MPA in the future.

References

[1] LI Z ZH, LUO C Y, YAO G , et al. Design of a concise and dual-band tunable metamaterial absorber [J]. Chinese Optics Letter, 2016 ,14(10):102303.

[2] ZHAO Z, SU S, ZHOU H, et al. "Fast" plasmons propagating in graphene plasmonic waveguides with negative index metamaterial claddings[J]. Nanomaterials, 2020,10(9):1637.

[3] LANDY N I, SAJUYIGBE S, MOCK J J, et al. Perfect metamaterial absorber[J]. Physical Review Letters , 2008,100(5):207402.

[4] TUAN T S , HOA N . Numerical study of an efficient broadband metamaterial absorber in visible light region[J]. IEEE Photonics Journal, 2019, 11(3):1-10.

[5] SCHURIG D, MOCK J J, JUSTICE B J, et al. Metamaterial electromagnetic cloak at microwave frequencies[J]. Science, 2006, 314(5801):977-980.

[6] WEN R M, LI L Y, HAN K W. A quick novel experimental method of metamaterial electromagnetic cloaking structure at microwave frequencies[J]. Acta Physica Sinica, 2010,59(7):4607-4611.

[7] ZHAO Y, HE Q P, HUANG J, et al. Ultrafast control of slow light in THz electromagnetically induced transparency metasurfaces[J]. Chinese Optics Letter, 2021, 19(7):073602.

[8] GUO C F, SUN T, CAO F, et al. Metallic nanostructures for light trapping in energy-harvesting devices[J]. Light Science & Applications, 2014, 3(4):e161.

[9] MUHARREM K, MEHMET B, EMIN U. Microwave energy harvesting based on metamaterial absorbers with multi-layered square split rings for wireless communications[J]. Optics Communication, 2017, 392(7):31-38.

[10] YOUNG J Y, JU S J Metamaterial absorber for electromagnetic waves in periodic water droplets[J]. Scientific Reports, 2015,5(9):14018.

[11] HE S L, CHEN T. Broadband THz absorbers with graphene-based anisotropic metamaterial films[J]. IEEE Transactions on Terahertz Science & Technology, 2013, 3(6):757-763.
[12] MOU N, LIU X, WEI T Large-scale, low-cost, broadband and tunable perfect optical absorber based on phase-change material[J]. Nanoscale, 2020,12(1):5374-5379.
[13] WEN D, YUE F, Li G. Helicity multiplexed broadband metasurface holograms[J]. Nature Communication 2015, 6(9): 8241.
[14] XIAO J Y, XIAO R W, ZHANG R X. Tunable terahertz absorber based on transparent and flexible metamaterial[J]. Chinese Optics Letter, 2020,18(9):092403.
[15] LIU J, MA W, CHEN W, et al. Numerical analysis of an ultra-wideband metamaterial absorber with high absorptivity from visible light to near-infrared[J] Optics Express, 2020, 28(16):23748-23760.
[16] LI M, MUNEER B, YI Z, et al. A broadband compatible multispectral metamaterial absorber for visible, near-infrared, and microwave bands[J]. Advanced Optical Materials, 2018, 6(9):1701238.
[17] KAI S, RIEDEL C A, URBANI A, et al. VO_2 thermo-chromic metamaterial-based smart optical solar reflector[J]. ACS Photonics, 2018,5(6):2280-2286.
[18] YUAN H, ZHU B O, FENG Y. A frequency and bandwidth tunable metamaterial absorber in x-band[J]. Journal of Applied Physics, 2015, 117(17):2083-1438.
[19] LIN B Q, ZHAO S H, WEI W, et al. Design of a tunable frequency selective surface absorber as a loaded receiving antenna array[J]. Chinese Physics B, 2014, 23(002):252-256.
[20] SU Z, YIN J, ZHAO X. Terahertz dual-band metamaterial absorber based on graphene/MgF2 multilayer structures[J]. Optics Express, 2015, 23(2):1679-1690
[21] LIU C, QI L, ZHANG X. Broadband graphene-based metamaterial absorbers[J]. AIP Advances, 2018, 8(1):015301.
[22] JEPSEN P U, FISCHER B M, THOMAN A, et al. Metal-insulator phase transition in a VO_2 thin film observed with terahertz spectroscopy[J]. Physical review. B, Condensed Matter and Materials Physics, 2006, 74(20):205103.
[23] KAKIUCHIDA H, JIN P, NAKAO S, et al. Optical properties of vanadium dioxide film during semiconductive - metallic phase transition[J]. Japanese Journal of Applied Physics, 2014, 46(5):L113-L116.
[24] LEI L, LOU F, TAO K. Tunable and scalable broadband metamaterial absorber involving VO2-based phase transition [J].Photonics Research, 2019,7(7):734-741.
[25] DAO R, KONG X, ZHANG H F, et al. A tunable ultra-broadband metamaterial absorber with multilayered structure[J]. Plasmonics, 2020, 15(6):1-7.
[26] JIANG X W, WU H. Metamaterial absorber with controllable absorption wavelength and absorption efficiency[J]. Acta Physica Sinica,70(2):027804.
[27] XU H X, HU L Z, LU Y X. et al. Dual-band metamaterial absorbers in the visible and near-infrared regions[J]. The Journal of Physical Chemistry C, 2019, 123(15):10028-10033.
[28] SMITH G, GENTLE A, ARNOLD M. Nanophotonics-enabled smart windows, buildingsand wearables [J]. Nanophotonics, 2016,5(1):55-73.
[29] LIU H, WANG Z H, LI L, et al. Vanadium dioxide-assisted broadband tunable terahertz metamaterial absorber[J]. Scientific Reports, 2019, 9(1):5751.
[30] JOHSON P, CHRISTY R. Optical constant of the noble metal[J]. Physical Review B, 1972,6(12):4370-4379.
[31] FAN F, HOU Y, JIANG Z W, et al. Terahertz modulator based on insulator-metal transition in photonic crystal waveguide[J]. Applied Optics, 2012, 51(20):4589-4596.
[32] DDING F, DAI J, CHEN Y T. Broadband near-infrared metamaterial absorbers utilizing highly lossy metals [J]. Scientific Reports, 2016,6(12):39445.
[33] DUAN X, CHEN S, LIU W, et al. Polarization-insensitive and wide-angle broadband nearly perfect absorber by tunable planar metamaterials in the visible regime[J]. Journal of Optics, 2014, 16(12):125107-125113.
[34] ZENG Z W, LIU H T, ZHANG S W. Design of extraordinary optical transmission refractive index sensor of subwavelength metallic slit array based on a fabry perot model[J].Acta Physica Sinica, 2012,61(20):200701.

Metamaterial Absorber with Tunable Absorption Bandwidth Based on Vanadium Dioxide

JIANG Xiaowei[1,3], WANG Sheng[1], WU Hua[2,3]

(1 *College of Information Engineering, Quzhou College of Technology, Quzhou, Zhejiang* 324000, *China*)

(2 *College of Physics and Electronic Information, GanNan Normal University, Ganzhou, Jiangxi* 341000, *China*)

(3 *Key Laboratory of Opto-electronics Technology Ministry of Education, Beijing University of Technology, Beijing* 100124, *China*)

Abstract: Metamaterial Perfect Absorber (MPA) is currently a research hotspot because of its numerous advantages such as high absorption efficiency, ultra-thin thickness, simple structure and so on. Since Landy et al. first proposed an MPA with perfect absorption characteristics, different types of MPAs have been proposed, and the absorption wavelengths over microwave, terahertz, infrared, and visible bands have been identified. However, once the structural parameters of MPA are fixed, the absorption bandwidth of MPA almost cannot be dynamically adjusted, which will limit its applications in some particular fields. This paper proposes a bandwidth-tunable MPA which is composed of vanadium dioxide (VO_2) and Au. The research group simulated and analyzed the MPA based on Finite Difference Time Domain (FDTD) method. In the simulation, a periodic boundary condition was added in x- and y-directions, and a perfect match layer was added in the z-direction as the boundary condition. The polarization of the incident light was set to be TM polarization (Along the x axis). Incident light was perpendicular to the surface of the structure, which indicated the incident angle θ is 0. The simulation results show that the tuning range of absorption bandwidth can achieve 0.378 μm by controlling the temperature of VO_2, and the absorption wavelength of MPA covered visible and near-infrared light. To explore the physical explanation for the high absorption efficiency in different wavelengths, we analyzed electromagnetic field distribution in MPA in different wavelengths, and revealed that although the high absorption efficiency is caused by the incident-light-stimulated surface plasmons in MPA, the working mechanism in visible and near infrared wavelength is quite different. In visible light range, no matter vanadium dioxide is in metallic state or dielectric state, the high absorption efficiency is caused by Propagating Surface Plasmon (PSP). On the other hand, for near-infrared light, if vanadium dioxide is in dielectric state, the high absorption efficiency is due to the Localized Surface Plasmon (LSP); or if vanadium dioxide is in metallic state, the high absorption efficiency is due to Fabry-Perot (FP) cavity resonance. Our results show that the MPA has the potential to be used in applications such as optical integrated devices and thermal emitters.

Key words: Metamaterial; Absorber; Tunable absorption bandwidth; Vanadium dioxide; Surface plasmon polariton

OCIS Codes: 160.3918; 120.5700; 120.4880